Nutrient availability in the North Pacific region not primarily driven by climate through the Quaternary

Andrea M. Snelling[1*], George E. A. Swann[1*], Vanessa Pashley[2], Jack H. Lacey[2], Matthew S.A. Horstwood[2], Melanie J. Leng[2, 3]

[1] School of Geography, University of Nottingham, Nottingham, NG7 2RD, UK

[2] National Environmental Isotope Facility, British Geological Survey, Keyworth, Nottingham, NG12 5GG, UK

[3] School of Biosciences, University of Nottingham, Sutton Bonington Campus, Loughborough, NE12 5RD, UK

* Corresponding author: andrea.snelling@nottingham.ac.uk, george.swann@nottingham.ac.uk

Keywords

North Pacific; Silicon isotope; biogeochemical cycling; nutrient utilisation; ocean stratification; Mid-Pleistocene Transition

Abstract

The subarctic North Pacific Ocean is a relatively understudied region in terms of palaeoclimate, limiting our understanding of how the region has both driven and responded to palaeoenvironmental events. Today, the subarctic North Pacific Ocean is marked by a year round stratified water column with a halocline at c. 300 m water depth. Previous studies at ODP Site 882 in the Northwest Pacific have suggested the stratified water column system developed at the onset of major Northern Hemisphere Glaciation (2.73 Ma). In addition to limiting the upwelling of carbon-rich deep waters and associated ventilation of CO_2 to the atmosphere, the shift to a stratified state fundamentally altered oceanographic conditions and biogeochemical cycling across the region. Key questions remain over whether the region was permanently stratified for all of the Quaternary, or whether the changes in stratification/biogeochemical cycling altered over major climatic transitions such as the Mid-Pleistocene Transition (MPT), a process that would alter regional ocean-atmospheric carbon exchanges. We present new silicon and oxygen isotope data from diatoms ($\delta^{30}Si_{diatom}$ and $\delta^{18}O_{diatom}$), alongside previously published data in order to test the mechanisms of biogeochemical cycling in the subarctic North Pacific Ocean between 2.85 Ma and 0.06 Ma, including influences from the wider region such as Glacial North Pacific Intermediate Water (GNPIW) originating in the Bering Sea. This has enabled us to reconstruct temporal changes in photic zone nutrient utilisation and silicic acid supply in the northwest subarctic Pacific Ocean through the progressive intensification of glacial-interglacial cycles through the Quaternary and over the MPT. We show that prior to the MPT climate does not appear to be a primary controller of nutrient availability in the North Pacific region, but that following the MPT, it has a greater influence, shown by the interrelationship with the upwelling index from the Bering Sea.

1. Introduction

The history of the subarctic north-west Pacific Ocean, has been relatively understudied compared to other marine locations due to the poor preservation of calcareous fossils. Over the past two decades, evidence has emerged as to the region's potential role as a driver of global climatic change through oceanic-atmospheric exchanges in CO_2. The area today (Figure 1) is marked by a year round stratified water column at c. 300 m water depth (Haug et al., 1999) as a result of a strong vertical salinity gradient (halocline). The halocline is considered to be generally stable (Swann et al., 2006) but recent studies using Argo profiling float data suggest that the halocline has distinct zonal patterns in terms of depth and intensity, with intensification of the halocline occurring in late winter (Katsura et al 2020). In the past, the absence of a halocline (e.g. during the Pliocene) would have allowed significant upwelling of nutrient and CO_2 rich deep water to the surface, helping to maintain the warm Pliocene climate state (Haug et al., 1999).

Although the development of the halocline at the onset of major Northern Hemisphere Glaciation (NHG) (2.73 Ma) inhibited the upwelling of this North Pacific Deep Water (NPDW) and helped lower atmospheric $p$$CO_2$ (Haug et al., 1999; Sigman et al., 2004; Haug et al 2005), the subsequent history of subarctic Pacific Ocean stratification is poorly constrained (Swann, 2010). There is evidence of periodic breakdowns in the halocline during the late Quaternary (Sarnthein et al., 2004; Jaccard et al., 2005, 2009, 2010; Galbraith et al., 2007, 2008; Gebhardt et al., 2008; Brunelle et al., 2010; Swann and Snelling, 2015), including the last deglaciation (Gray et al., 2018, Rae et al., 2020), but there are few data relating to the intervening period. Any changes in stratification will have affected the biological pump, which is responsible for the removal of nutrients and CO_2 from the surface waters into the ocean interior and plays a vital role in regulating the climate through ocean/atmosphere interactions (Sigman and Hain, 2012).

In addition to the halocline, recent work has also pointed to the role of Glacial North Pacific Intermediate Water (GNPIW) in controlling North Pacific Deep Water (NPDW) upwelling and consequently releases of CO_2 to the atmosphere during glacials over the past 1.2 Ma (Knudsen and Ravello 2015a, Worne et al 2019, 2020). GNPIW is a dense water mass formed as a result of brine rejection during winter sea ice production in the Bering Sea (Warner and Roden, 1995, Shcherbina et al., 2003), taking atmospherically equilibrated oxygen to the ocean interior (Knudson and Ravello, 2015a). It is thought to propagate southwards into the open ocean through the Kamchatka Strait (Horikawa et al., 2010, Jang et al., 2017) and further limits NPDW upwelling and primary productivity in surface waters (Worne et al., 2019, 2020) (Figure 2). The name GNPIW distinguishes this water from NPIW which originates in the Sea of Okhotsk and then spreads eastwards into the North Pacific towards the California current region (Max et al., 2014).

Currently, the long-term evolution of the subarctic Pacific halocline, the expansion of GNPIW/NPIW into the subarctic Pacific and their combined impact on nutrient dynamics through the early Quaternary is poorly understood. Constraining these changes is key, not only to understand the timing of NPDW upwelling and release of CO_2 to the atmosphere, but also the role of nutrient availability and the biological pump in mediating such activity and exporting carbon from the photic zone (productivity zone above the halocline) into the deep ocean/sediment record (Volk and Hoffert, 1985; Sigman et al., 2010). In particular, the role and response of the subarctic Pacific Ocean over the Mid-Pleistocene Transition (MPT) (1.25-0.7 Ma) remains unclear, although recent studies in the Bering Sea have begun to address this (Worne et al., 2019, 2020). The MPT marks a significant change in Earth's climate history as the glacial-interglacial cycles migrate from small-amplitude 41 ky cycles to a dominance of larger amplitude, asymmetric 'saw-tooth' 100 ky glacial-interglacial cycles. Climate records suggest that there were no significant shifts in solar radiation as a result of orbital variations to cause this change in glacial periodicity, but instead the climate system developed an enhanced sensitivity to orbital forcing at this time (Ravelo et al., 2004, Mc Clymont et al., 2013). The internal mechanisms and teleconnections behind the transition from 41 ky to 100 ky glacial-interglacial cycles are still much debated (McClymont et al., 2013) and include a threshold response to atmospheric CO_2 concentrations (Raymo, 1997), a change in global ice sheet dynamics (Clark and Pollard, 1998; Raymo et al., 2006; Crowley and Hyde, 2008), and other feedbacks related to deep-water cooling, thermocline depth, sea-ice distributions and atmospheric circulation (Tziperman and Gildor, 2003; McClymont and Rosell-Melé, 2005; Lee and Poulsen, 2006; McClymont et al., 2013, Kender et al. ,2018, Worne et al., 2020).

Here we present diatom oxygen and silicon isotope data ($\delta^{18}O_{diatom}$ and $\delta^{30}Si_{diatom}$) from ODP Site 882, alongside previously published data sets from the Late Quaternary (Swann and Snelling 2015) and Late Pliocene/Early Quaternary (Swann 2010, Bailey et al., 2011). Changes in $\delta^{18}O_{diatom}$ can be used to reflect changes in oceanographic conditions (ocean mass, fresh water, temperature) including changes in stratification state, whilst $\delta^{30}Si_{diatom}$ records changes in productivity linked to photic zone silicic acid utilisation, which is dependent on the supply and biological demand for silicic acid (Reynolds et al., 2006). These data are used to investigate the relationship between changes in the biological pump, GNPIW/NPIW propagation and halocline stratification in the north-west subarctic Pacific through the Quaternary and over the MPT.

2. Material and methods

ODP Site 882 is situated on the western section of the Detroit Seamounts at a water depth of 3,244m (50°22′ N, 167°36′ E) (Figure 1). The age model for this core comes from astronomically calibrated high-resolution gamma-ray attenuation porosity evaluator (GRAPE) density and magnetic susceptibility measurements (Tiedemann and Haug, 1995). The period from 0-0.8 Ma is then refined using higher resolution benthic foraminifera $\delta^{18}O$ that corroborate the tuned stratigraphy and by visually matching common inflection points between ODP Site 882 biogenic barium data and EPICA Dome C δD (Jaccard et al., 2005, 2009, 2010).

Sixty-six samples from ODP Site 882 between the ages of 0.48 and 2.48 Ma were prepared for diatom isotope analysis. Samples were chosen to encompass both glacial and interglacial periods through the Quaternary and were cleaned using a combination of heavy liquid separation, hydrogen peroxide and hydrochloric acid (Swann et al., 2013). Samples were further sieved at 53 µm and 20 µm to remove sponge spicules and radiolaria, which may have different isotopic fractionation factors to diatoms (e.g. de la Rocha, 2003, Snelling et al., 2014, Cassarino et al., 2018), and checked using a Zeiss Axiovert 40 C inverted microscope, scanning electron microscope, and X-ray fluorescence to confirm sample purity and the absence of non-diatom contaminants. Samples with an XRF Al/Si ratio of ≤ 0.03% were retained for isotope analysis (Figure 3). Previous studies have considered the impact of species effects on both $\delta^{18}O_{diatom}$ and $\delta^{30}Si_{diatom}$ (Swann et al., 2008, Maier et al 2013, Grasse et al., 2021) and indicate that detailed assemblage data is useful in interpreting isotope data. Here, all samples contained a variety of similar diatom species, often broken up therefore we consider any species effects to be negligible.

Samples were digested and prepared for $\delta^{30}Si_{diatom}$ analysis following methods outlined in Panizzo et al. (2016) To overcome any analytical bias, sample and reference materials are acidified using HCl (to a concentration of 0.05M, using twice quartz-distilled acid) and sulphuric acid (to a concentration of 0.003M, using Romil Ultra Purity Acid and all samples are doped with ~300ppb magnesium (Mg, Alfa Aesar SpectraPure) to correct for the effects of instrument induced mass bias, (Hughes, 2011). Analyses were carried out on a ThermoScientific Neptune Plus MC-ICP-MS (multi collector inductively coupled plasma mass spectrometer) at the National Environmental Isotope Facility (NEIF) at the British Geological Survey (UK), operated in wet plasma mode using the method/settings outlined in Cockerton et al. (2013) and Panizzo et al. (2016). In brief, the data are acquired using a dynamic, two sequence, acquisition. Faraday amplifier gains are measured at the beginning of each analytical session and data are collected as 1 block of 20 ratios measured at 16.8 second integrations for Si and 8.4 seconds for Mg. The blank contribution is measured on the sample make-up acid (0.05M HCl, 0.003M H_2SO_4) using a shortened version of the acquisition procedure. An on-line background correction is made, with the values obtained for the blank acid subtracted from the succeeding sample.

NBS-28 is employed as the primary reference material and Diatomite as the validation material; both of which are analysed repeatedly during each analytical session.

$\delta^{18}O_{diatom}$ was obtained using a step-wise fluorination method also at the NEIF with measurements made on a Thermo Finnigan MAT 253 and values converted to the VSMOW scale using the NEIF within-run laboratory diatom standard BFC_{mod} which has been calibrated against NBS28 (Leng and Sloane, 2008). Analytical error is 0.3‰ (1σ) for oxygen analysis (Leng and Sloane, 2008) and 0.15‰ (2σ) for silicon.

2.1 Silicon isotope fractionation

Silicon isotope fractionation by organisms can occur within a closed or open system. In an 'open' system, under steady state conditions, there is a continuous supply of nutrients to the photic zone, whereas in a closed system the supply of nutrients is finite and fractionation occurs along a Rayleigh distillation curve. Historically, it has been accepted that following the onset of major NHG at 2.73 Ma, the formation of the halocline was a permanent feature of the subarctic North Pacific Ocean and its presence would suggest that the area is representative of a closed system given that the halocline restricts mixing between deep and surface water (productivity zone), thus creating an environment with a finite supply of nutrients. In this case changes in $\delta^{30}Si_{diatom}$ can be represented by:

$$\delta^{30}\mathrm{Si}_{\mathrm{diatom}} = \delta^{30}\mathrm{Si(OH)}_{4\ \mathrm{initial}} - \varepsilon \bullet (f \ln f \,/(1-f)) \qquad \text{(Eq. 1)}$$

where $\delta^{30}Si(OH)_{4\ initial}$ is initial silicic acid in the surface water (derived from NPDW), ε is the fractionation factor between the dissolved and particulate phase [–1.1‰: De la Rocha et al (1997)] and f is the fraction of silicic acid remaining in the surface ocean. In the subarctic Pacific, Reynolds et al (2009) use a mean value of 1.63‰ for surface water in their models because the Si isotope value is not fixed or homogenized at the surface and is the value that we use here for $\delta^{30}Si(OH)_4$ $_{initial}$ () We assume that this value has not changed over time. Silicic acid utilisation can then be calculated as (1 – *f*).

With $\delta^{30}Si_{diatom}$ a function of both nutrient utilisation and supply to the photic zone, changes in the supply of silicic acid can be calculated relative to the oldest sample referred to in this study (2.85 Ma) by normalising rates of nutrient utilisation against opal/biogenic rates of siliceous productivity (Horn et al., 2011):

$$\mathrm{Si(OH)}_{4(\mathrm{supply})} = \frac{\mathrm{Opal}_{\mathrm{sample}}/\mathrm{Opal}_{2.85\ \mathrm{Ma}}}{\mathrm{Si(OH)}_{4(\mathrm{utilisation\ sample})}/\mathrm{Si(OH)}_{4(\mathrm{utilisation\ 2.85\ Ma})}} * \frac{\mathrm{Si(OH)}_{4\,\mathrm{Deep}}^{\mathrm{Present}}}{\mathrm{Si(OH)}_{4\,\mathrm{Deep}}^{\mathrm{Sample}}} \quad (\mathrm{Eq.}\ 2)$$

The oldest sample was chosen to normalise the data as this is prior to the formation of the halocline and represents an open ocean system, when nutrient supply and productivity would have been high. Using the above equations, silicic acid utilisation and supply was calculated for the new samples measured in this study as well as for the previously measured samples from the Late Quaternary (Swann and Snelling 2015) and from the Late Pliocene/Early Quaternary (Swann 2010, Bailey et al., 2011). For $Si(OH)_{4\ Present\ Deep}$ we use the modern subarctic Pacific value at 1,500 m of 174.2 µM (Reynolds et al., 2006) and we assume that past $Si(OH)_4$ concentrations were the same as today. Opal (%wt) data is an amalgamation of existing data from Tiedermann and Haug (1995), Haug et al., (1995) and Jaccard et al., (2005, 2009, 2010), in addition to new data from this study measured on freeze dried sediment samples, following wet alkaline digestion and UV/VIS spectrophotometry. Where required, opal values for individual samples were obtained by linear interpolation from the combined opal datasets.

2.2 Oxygen isotope correction

To ensure that changes in $\delta^{18}O_{diatom}$ reflect local surface oceanographic conditions, all values from this study and existing $\delta^{18}O_{diatom}$ values (Swann and Snelling 2015, Swann, 2010, Bailey et al., 2011) were corrected for whole ocean changes in $\delta^{18}O$ using the LR04 benthic foraminifera $\delta^{18}O$ dataset (Lisiecki and Raymo, 2005). In addition, changes in sea surface temperature (SST) were corrected relative to the temperature of the oldest sample at 2.85 Ma, using U^{k}_{37} SST reconstructions from ODP Site 882 (Haug et al., 2005) with a $\delta^{18}O_{diatom}$ temperature coefficient of –0.2‰/°C (Brandriss et al., 1998; Moschen et al., 2005).

3. Results

3.1 $\delta^{30}Si_{diatom}$

Over the presented interval (0.06-2.85 Ma), there are significant changes in $\delta^{30}Si_{diatom}$ with values fluctuating between 0.5 ‰ and 1.7 ‰ (Figure 4). Fluctuations occur throughout the record with the biggest changes occurring around 0.06-0.15 Ma, 0.54-0.62 Ma, 0.92-1.0 Ma, 1.19-1.26 Ma, 1.54-1.64 Ma and 2.56-2.75 Ma. The lowest $\%Si(OH)_{4\ utilisation}$ values occur following NHG (2.55-2.60 Ma), with subsequent fluctuations predominantly in interglacial periods. There are fewer isotope data between 1.63 Ma and 2.48 Ma due to the low opal concentrations and poor diatom preservation over this period. The intervals of high fluctuation occur when there is variable opal concentration (Figure 4), but there is no firm relationship between $\delta^{30}Si_{diatom}$ and opal (r^2 = 0.05). Between 0.06 Ma – 0.2 Ma $\%Si(OH)_{4\ utilisation}$ drops to values similar to the start of the Quaternary.

The supply of silicon to the photic zone follows changes in opal concentrations, with peaks in supply at 0.12 Ma, 0.70-0.71 Ma, 0.84-1.05 Ma, 1.23-1.26 Ma, 1.45-1.59 Ma and 2.6 Ma. Comparison of the $\%Si(OH)_{4\ utilisation}$ and $Si(OH)_{4\ supply}$ show little relationship with high and low utilisation occurring under both high and low nutrient supply (Figure 5b) (R^2 = 0.001). Silicon supply and utilisation were also calculated under an open system scenario, to constrain silicon dynamics in an unstratified water column state, and we found similar trends in the data (see supplementary data). This means that if the ocean state did change to an open system during the Quaternary, the closed system trends reported in this study remain valid.

3.2 $\delta^{18}O_{diatom}$

The $\delta^{18}O_{diatom}$ record has distinct peaks over the analysed interval, with values fluctuating between 46.2‰ and 34.5‰ (Figure 4). The biggest changes occur at 0.07-0.11 Ma, 0.92-0.96 Ma, 1.05-1.26 Ma, 2.28-2.40 Ma, 2.4-2.28 Ma and 2.63-2.69 Ma, with high and low values apparent in both glacial and interglacial periods. The SST normalised $\delta^{18}O_{diatom}$ values show that despite the significant change in temperature over the analysed interval (between 1.8 and 18.2°C), this can only account for up to 3.3‰ of the change in $\delta^{18}O_{diatom}$, based on a $\delta^{18}O_{diatom}$ temperature coefficient of –0.2‰/°C (Brandriss et al., 1998; Moschen et al., 2005). Therefore, the range of $\delta^{18}O_{diatom}$ (up to 11.7‰) is evidence of significant changes in photic zone seawater $\delta^{18}O$ at ODP Site 882.

4. Discussion

Marine diatoms are responsible for up to 70% of primary productivity (Nelson et al., 1995) and play an important role in organic carbon export production (Smetacek 1999). Consequently, considering the supply and utilisation of nutrients by diatoms provides an indication of the strength of the past biological pump and ocean-atmospheric exchanges of CO_2. The modern North Pacific Ocean is a high-nitrate, low-chlorophyll region (HNLC) and as such diatom/opal productivity can be limited by iron (Fe) and light (Tsuda et al., 2003, Lam et al., 2013; Wang et al., 2019). The delivery of Fe to the subarctic Pacific may have changed on glacial-interglacial timescales (Kohfeld and Chase, 2011). Productivity is also linked to regional ocean stratification (halocline) and the presence/absence of GNPIW/NPIW in this region, which impedes the upwelling of nutrient rich NPDW. Worne et al. (2019, 2020) created an upwelling index for the Bering Sea, finding that decreased upwelling and nutrient availability during glacial periods was a result of increased sea ice and GNPIW formation. Further comparisons have shown a correlation between changes in subarctic Pacific opal concentrations at ODP Site 882 and Bering Sea upwelling (Worne et al., 2019, 2020) with broadly similar interglacial peaks 0.48-0.8 Ma, but less association for the remaining record. This suggests that the influence of Bering Sea GNPIW in the wider subarctic North Pacific is variable and that prior to 1 Ma, climate does not play a primary role in either nutrient availability or GNPIW formation in the North Pacific Ocean, given the disassociation between the climate cycles and the upwelling peaks at this time. The role of the halocline, however, may have had a greater influence on nutrient availability.

Diatom/opal concentrations in the ocean sedimentary record are also influenced by export production and preservation. Following the collapse in biogenic opal concentrations at 2.73 Ma in the North Pacific (Haug et al., 1999) and opal deposition to other areas (Cortese et al., 2004), Quaternary opal concentrations generally remained low, but show significant peaks (1.53 Ma, 1.28 Ma, 1.04 Ma, 0.91 Ma, 0.71 Ma) (%BSi Figure 4) indicating enhanced productivity and/or favourable opal preservation in the North Pacific (Haug et al., 1995; Jaccard et al., 2010). The degree to which GNPIW/NPIW and the halocline played a role in controlling upwelling and export production at ODP Site 882 can be investigated using the silicic acid supply and utilisation data calculated from $\delta^{30}Si_{diatom}$ and their inter-relationships. These data can constrain the activity and efficiency of the silicon and biological pump to provide insight to the contribution of the region to influencing/regulating global climate change, through ocean/atmosphere exchanges of CO_2.

4.1 Early Quaternary records

Following the NHG at 2.73 Ma opal productivity in the photic zone dropped from an average of 66 %wt (2.74-3 Ma) to 19 %wt (0-2.73 Ma) which has been attributed to the formation of the halocline, limiting upwelling of nutrients from deep water into the photic zone (Haug et al., 2005). From 2.73-2.55 Ma, previously published records (Bailey et al., 2011) suggested that an increase in iron deposition raised the biological demand for nitrate relative to silicic acid (Figure 5A), accompanied by a change in the ratio of nutrients supplied to the photic zone, which led to under-utilisation of silicic acid, reflected in the $\%Si(OH)_{4\ utilisation}$ shown here and a corresponding increase in nitrate utilisation (Figure 5A). Our calculations of $Si(OH)_{4\ supply}$ show the supply of silicic acid to the photic zone over this period is extremely variable (2.53-2.63 Ma) and shows distinct peaks compared to the levels experienced prior to NHG (Figure 5A), which suggests that changes in supply of silicic acid may be driving the changes in $\%Si(OH)_{4\ utilisation}$ at this time, rather than Fe limitation. Our data suggests that the general decrease in silicic acid utilisation is accompanied by a variable but significant increase in $Si(OH)_{4\ supply}$, although the source of this is not clear. Previous work has discussed the role of ice sheets on the global silicon cycle and suggested that ice sheets could have delivered large quantities of isotopically light silica to the oceans during periods of enhanced glacial activity (Hawkings et al., 2017). At the same time, large fluctuations in $\delta^{18}O_{diatom}$ of c. 5 ‰ at 2.67 Ma are attributed to freshwater input from glacial meltwater (Swann, 2010), suggesting the enhanced peaks in $Si(OH)_{4\ supply}$ may originate from the same glacial source.

The large changes in the supply of silicic acid to the photic zone and variable (although declining) $\%Si(OH)_{4\ utilisation}$, variable $\delta^{15}N$, accompanied by an increase in BSi (%wt), following the initial crash at 2.73 Ma would indicate potential differences in water column conditions. There is an evident influx of meltwater as indicated by the changes in $\delta^{18}O_{diatom}$, and potentially $Si(OH)_{4\ supply}$ as well as some form of nutrient limitation affecting $\%Si(OH)_{4\ utilisation}$ nitrate utilisation, although these changes are not synchronous (Figure 5A). By 2.48 Ma, there is a return to complete utilisation of silicic acid and a drop in silicic acid supply, indicating a more established stratified ocean. Between 2.40-2.48 Ma there is a significant freshening to the photic zone, indicated by a > 8 ‰ drop in $\delta^{18}O_{diatom}$, accompanied by a drop in opal productivity from 40% to close to zero and enhanced ice-rafted debris IRD deposition (Bailey et al., 2011), which could relate to a further intensification of NHG, similar to 2.73 Ma. By 2.28 Ma $\delta^{18}O_{diatom}$ has increased by > 10 ‰ (Figure 5A) to levels similar to the Pliocene and suggests a decreased input of meltwater at a time of enhanced nutrient utilisation under a relatively reduced supply. It has previously been suggested that the region acted as a net sink for CO_2 following NHG and the formation of the halocline (Swann et al., 2018). The changes in our $\%Si(OH)_{4\ supply}$ and $\%Si(OH)_{4utilisation}$ data over this period however, suggests variable efficiency in the biological pump at a time of instability in palaeoceanographic conditions, given the dramatic changes in $\delta^{18}O_{diatom}$, (Figure 5A).

4.2 Middle Quaternary and the MPT

In the middle Quaternary, prior to the MPT (1.38-1.64 Ma Figure 5B), there is significant variation in siliceous productivity, silicic acid supply and utilisation. Our results show reduced consumption of nutrients is linked to both enhanced and reduced nutrient supply but predominantly generally low productivity. Over MIS 51-52 (1.51-1.53 Ma) utilisation is high yet opal productivity varies significantly (between 5 and 66%). Our supply data indicates an increase in the supply of nutrients during the interglacial (MIS 51), corresponding to a productivity peak (Figure 5B). Complete consumption of nutrients at times of enhanced productivity and nutrient supply would be similar to pre-NHG times when there was unimpeded deep water upwelling, as has been suggested for more recent records from this area (MIS 5b/c: Swann and Snelling, 2015, MIS 2 Okazaki et al., 2010).

Our $\delta^{30}Si_{diatom}$ record and associated utilisation and supply data over the MPT are not noticeably different to the Early Quaternary in terms of variability, however the inter-relationships between productivity, supply and utilisation of nutrients does vary as discussed below. There are two distinct excursions in the nutrient utilisation record (1.54-1.60 Ma and 0.93-1.0 Ma), and productivity and supply are slightly enhanced over this period, such that mean opal wt% = 26% over the MPT and 13% pre-MPT. At the onset of the MPT, 1.25 Ma, productivity and nutrient supply are enhanced, whilst utilisation is slightly reduced and $\delta^{18}O_{diatom}$ is at similar levels to the Pliocene (Figure 5B). Reduced utilisation during periods of increased supply have previously been linked in part to iron flux contributing to nutrient limitation (Bailey et al., 2011). Here, the scale of change compared to the period immediately following the onset of NHG, however, is much smaller and short lived. Worne et al., (2020) have indicated reduced upwelling over the MPT in the Bering Sea, controlled by sea ice extent and the expansion of GNPIW into the wider subarctic region and that prior to the middle MPT (0.9 Ma) other/additional factors were controlling nutrient upwelling. The enhanced nutrient supply and productivity reported here suggest GNPIW may not have reached this far south at this time and that nutrient supply may have been more affected by a reduction in the strength of the halocline. The reduced utilisation under such conditions would indicate a less efficient biological pump.

Following the initial MPT opal high, our record shows a decrease in productivity and silicon supply, coupled with 4.4‰ drop in $\delta^{18}O_{diatom}$ and a rise in nutrient utilisation (1.24-1.16 Ma, MIS 37-35) (Figure 5B). It has previously been discussed that large changes in $\delta^{18}O_{diatom}$ are indicative of a freshening from meltwater and precipitation that could affect stratification and prevent upwelling of deeper water and thus nutrients. This could have led to a return to stratified conditions (halocline and potentially GNPIW) with complete utilisation of the available nutrients. It is also at this time that there is an evident change in the LR04 record (Lisecki and Raymo 2005) transitioning to 100 kyr cycles becoming more evident.

This pattern of enhanced supply and productivity and reduced utilisation, prior to a drop in $\delta^{18}O_{diatom}$ is similar to the period in the early Quaternary, where it was suggested that palaeoceanographic conditions may have been more unstable and the role of glacial meltwater could have had an effect on the supply of nutrients to the photic zone. The variability at this time is less pronounced than earlier in the Quaternary and could indicate that any weakening in the halocline was minimal and/or short lived.

The modern day halocline is preserved through high precipitation and low evaporation (Emile-Geay et al., 2003) but it is unlikely that the freshening at MIS 37-35 is solely a result of increased precipitation. Freshwater input to the surface waters could also be a result of glacial melt water, which for this region is likely to originate from the Bering Sea (Swann 2010, Kotilainen and Shackleton, 1995; McKelvey et al., 1995; St John and Krissek, 1999) as there is a pronounced seasonal advance and retreat of sea ice at this time (Detlef et al., 2018). It is possible that there were other sources of meltwater to this region including the Sea of Okhotsk, where proxy records indicate similarities in sea surface temperature change to the North Pacific (Lattaud et al., 2019) and the Kamchatka-Koryak coast which has been suggested as a source of meltwater to this area for the Late Quaternary (McCarron et al., 2021). IRD records from the Sea of Okhotsk suggest however, that it is a less likely source (McKelvey et al., 1995; St John and Krissek, 1999). Lam et al. (2013) showed from various proxy records that there was a productivity peak in the North Pacific at 14.5 kyr following deglaciation, with a subsequent freshening of surface waters, enhancing stratification in the upper ocean waters due to shutting down of relatively deep ocean convection. Swann and Snelling (2015) however show that freshwater acts as a secondary control on re-establishing ocean stratification and suggest that other factors including linkages to the Southern Ocean could be driving ocean stratification (Jaccard et al., 2005, 2010, Sigman et al., 2010, 2021. We are unable to discern whether the freshwater input is a primary or secondary factor affecting upwelling at this time.

The upwelling index from the Bering Sea indicates an upwelling high in the middle of MIS 35, whist our productivity and supply in the subarctic Pacific are in general decline following peaks in productivity in the preceding interglacial (MIS 37). There is no available upwelling data for MIS 37, but for MIS 35 it would suggest that there were different controls influencing upwelling between the two regions and that Bering Sea meltwater was not acting as a major influence on upwelling in the North Pacific Ocean at this time. The decrease in productivity over MIS 37-35 recorded in our data is in contrast to the findings of Diester-Haas et al. (2018), where an increase in productivity is linked to (but not driving) the sequestration of CO_2. The decrease in our proxy data is of a similar magnitude to conditions at the onset of NHG for the North Pacific (Haug, 1995, Reynolds et al., 2008, Swann, 2010, Bailey et al., 2011) and the formation of the halocline. Over MIS 37-35, our data highlights the sensitivity of the North Pacific region to stratification, which we suggest occurs at this time.

From 1-0.9 Ma (MIS 30-23), productivity is highly variable and shows no link to glacial/interglacial cycles. Utilisation is also variable, but enhanced supply of nutrients is often associated with high productivity. Low utilisation is associated with moderate to enhanced supply of nutrients and productivity over both glacial and interglacial cycles. Compared to the Bering Sea upwelling index, our productivity and supply data show some broad similarities, suggesting that GNPIW may be having more of an influence on North Pacific Ocean stratification at this time. This may be linked to closure of the Bering Strait (Kender et al., 2018, Worne et al., 2019, 2020,) and an increase in sea ice extent, which may have forced a greater link with the North Pacific Ocean.

4.3 Late Quaternary records

From the end of the MPT (0.7 Ma) to 0.48 Ma (MIS 18-13 Figure 5C) productivity peaks are predominantly associated with interglacials and enhanced supply but irregular consumption. In addition, productivity peaks are more closely aligned with the Bering Sea upwelling index (Worne et al., 2019), suggesting GNPIW during glacial periods in the North Pacific Ocean and upwelling during interglacial periods and an apparent link between climate change and productivity across the North Pacific region.

Records from 0.2-0.06 Ma (MIS 7-4 Figure 5D) show a greater range of variability in nutrient supply and utilisation than over the MPT, accompanied by a significant oceanic freshening (Swann and Snelling, 2015), which is suggested to have a strong influence on ocean stratification and the strength of the halocline. Nutrient productivity and supply appear to correspond with the Bering Sea upwelling index, indicating a continued alignment between the Bering Sea and the wider North Pacific region. Previous studies have indicated a strong link between the biogeochemistry of the North Pacific Ocean and climate (Jaccard et al., 2010, Knudson and Ravelo 2015b, Worne et al., 2020) and that the opening/closing of the Bering Strait would have had a strong influence on the formation of GNPIW, following the MPT (Worne et al., 2020).

5. Conclusions

Over the analysed interval our proxy data suggests that the North Pacific Ocean may have undergone changes in the strength of the ocean stratification throughout the Quaternary period as a result of weakening in the halocline and/or influence of GNPIW/NPIW. A number of factors likely influenced the changing ocean state, to varying degrees, over time however it would appear that prior to MIS 21, climate change and glacial-interglacial cycles were not driving productivity changes in this region and that factors influencing the Bering Sea did not impact the North Pacific Region in the same way. Between MIS 21-13 and MIS 7-4, climate and the influences of GNPIW did affect the North Pacific Ocean state, indicating a greater influence from the Bering Sea region.

Nutrient use and supply also do not appear to have been driven by climate change but are influenced by other factors that we are unable to quantify from our data. They do however show periods of a highly efficient biological pump (high productivity, high supply, complete consumption), which would have reduced any exchange of CO_2 with the atmosphere and may have served to sequester CO_2 deep in the ocean. Our data also show periods of inefficiency (high productivity, high supply, incomplete consumption) when the region may have acted as a source of CO_2 to the atmosphere. These periods of lower consumption in periods of higher productivity and supply require further investigation along with other proxy evidence. Modelling experiments have shown that a breakdown in stratification in the North Pacific is capable of producing a 30 ppm rise in atmospheric CO_2 (Rae et al., 2014). This is not insignificant and if a breakdown in stratification was more of a regular feature in the North Pacific Ocean over the Quaternary, then the role of this region in regulating global climate may have been previously underestimated and requires further clarification.

Acknowledgements

This research was funded through a Daphne Jackson Research Fellowship for AS (2017-2019). The $\delta^{30}Si$ and $\delta^{18}O$ analyses were completed through funding provided by the NERC Isotope Geosciences Facilities Steering Committee grant IP-1786-1117 (to GEAS). We are grateful to the International Ocean Discovery Program, including the crew on ODP Leg 145 for collecting the

samples from Site 882 and the Texas Core Repository curators. AS completed all of the sample preparation, ran the $\delta^{30}Si$ analysis with VP and led the writing of the manuscript. JL ran the analysis of $\delta^{18}O$ on prepared sample material. All authors contributed to the writing and interpretation of the manuscript.

References

Bailey, I., Q. Liu, G. E. A. Swann, Z. Jiang, Y. Sun, X. Zhao, and A. P. Roberts 2011, Iron fertilisation and biogeochemical cycles in the sub-Arctic northwest Pacific during the late Pliocene intensification of Northern Hemisphere glaciation, Earth Planet. Sci. Lett., 307(3–4), 253–265, doi:10.1016/j.epsl.2011.05.029

Brandriss, M. E., O’Neil, J. R., Edlund, M. B., and Stoermer, E. F. 1998, Oxygen isotope fractionation between diatomaceous silica and water, Geochim. Cosmochim. Ac., 62, 1119–1125.

Brunelle, B. G., Sigman, D. M., Jaccard, S. L., Keigwin, L. D., Plessen, B., Schettler, G., Cook, M. S., and Haug, G. H. 2010, Glacial/interglacial changes in nutrient supply and stratification in the western subarctic North Pacific since the penultimate glacial maximum, Quaternary Sci. Rev., 29, 2579–2590.

Cassarino ,L., Coath, C.D., Xavier, J. R., and Hendry, K. R. 2018, Silicon isotopes of deep sea sponges: new insights into biomineralisation and skeletal structure Biogeosciences, 15 (22).

Clark, P.U., Pollard, D., 1998. Origin of the middle Pleistocene transition by ice sheet erosion of regolith. Paleoceanography 13, 1–9.

Cockerton, H.E., Street-Perrott, F.A., Leng, M.J., Barker, P.A., Horstwood, M.S.A., Pashley, V., 2013. Stable-isotope (H, O, and Si) evidence for seasonal variations in hydrology and Si cycling from modern waters in the Nile Basin: implications for interpreting the Quaternary record. Quaternary Science Reviews 66, 4–21.

Cortese, G., R. Gersonde, C.-D. Hillenbrand, and G. Kuhn, 2004, Opal sedimentation shifts in the World Ocean over the last 15 Myr, Earth Planet. Sci. Lett., 224, 509–527

Crowley, T.J., Hyde, W.T., 2008. Transient nature of late Pleistocene climate variability. Nature 456, 226–230.

de La Rocha, C.L., Brzezinski, M.A., DeNiro, M.J., 1997. Fractionation of silicon isotopes by marine diatoms during biogenic silica formation. Geochim. Cosmochim. Acta 61, 5051–5056.

de la Rocha, C. L. 2003, Silicon isotope fractionation by marine sponges and the reconstruction of the silicon isotope composition of ancient deep water, Geology, 31, 423‑426.

Detlef, H., Belt, S.T., Sosdian, S.M., Smik, L., Lear, C.H., Hall, I.R., Cabedo-Sanz, P., Husum, K., Kender, S., 2018. Sea ice dynamics across the Mid-Pleistocene tran-sition in the Bering Sea. Nat. Commun.9. https://doi .org /10 .1038 /s41467 -018 -02845 -5.

Diester-Haass, L., Billups, K., Lear, C., 2018, Earth-science reviews productivity changes across the mid-Pleistocene climate transition Earth-Sci. Rev., 179, pp. 372-391, 10.1016/j.earscirev.2018.02.016

Emile-Geay, J., Cane, M. A., Naik, N., Seager, R., Clement, A. C., and van Green, A. 2003, Warren revisited: atmospheric freshwater fluxes and “Why is no deep water formed in the North Pacific”, J. Geophys. Res., 108, 3178, doi:10.1029/2001JC001058.

Galbraith, E.D., Jaccard, S.L., Pedersen, T.F., Sigman, D.M., Haug, G.H., Cook, M., Southon, J.R., Francois, R., 2007. Carbon dioxide release from the North Pacific abyss during the last deglaciation. Nature449, 890–893. https://doi .org /10 .1038 /nature06227.

Galbraith, E.D., Kienast, M., Jaccard, S.L., Pedersen, T.F., Brunelle, B.D., Sigman, D.M., Kiefer, T., 2008. Consistent relationship between global climate and surface ni-trate utilisation in the western subarctic Pacific throughout the last 500 ka. Paleoceanography23, 1–11. https://doi .org /10 .1029 /2007PA001518.

Gebhardt, H., Sarnthein, M., Grootes, P. M., Kiefer, T., Kuehn, H., Schmieder, F., and Rohl, U. 2008 Paleonutrient and productivity records from the subarctic North Pacific for Pleistocene glacial terminations I to V, Paleoceanography, 23, PA4212, doi:10.1029/2007PA001513.

Gray, W.R., Rae, J.W.B., Wills, R.C.J., Shevenell, A.E., Taylor, B., Burke, A., Foster, G.L., Lear, C.H., 2018. Deglacial upwelling, productivity and CO2outgassing in the North Pacific Ocean. Nat. Geosci.11, 340–344. https://doi .org /10 .1038 /s41561 -018 -0108 -6.

Haug, G.H., Maslin, M.A., Sarnthein, M., Stax, R., Tiedemann, R., 1995. Evolution of northwest Pacific sedimentation patterns since 6 Ma (Site 882). In: Rea, D.K., Basov, I.A., Scholl, D.W., Allan, J.F. (Eds.), Proceedings of the Ocean Drilling Program. Scientific Results. Ocean Drilling Program, College Station, TX, pp. 293–314.

Haug, G. H., D. M. Sigman, R. Tiedemann, T. F. Pedersen, and M. Sarnthein, 1999, Onset of permanent stratification in the subarctic Pacific Ocean, Nature, 401, 779–782.

Haug, G. H., Ganopolski, A., Sigman, D. M., Rosell-Mele, A., Swann, G. E. A., Tiedemann, R., Jaccard, S, Bollmann, J., Maslin, M. A., Leng, M. J., and Eglinton, G. 2005 North Pacific seasonality and the glaciation of North America 2.7 million years ago, Nature, 433, 821–825.

Horikawa, K., Asahara, Y., Yamamoto, K., Okazaki, Y., 2010. Intermediate water formation in the Bering Sea during glacial periods: evidence from neodymium isotope ratios. Geology38, 435–438. https://doi .org /10 .1130 /G30225 .1.

Horn, M. G., C. P. Beucher, R. S. Robinson, and M. A. Brzezinski., 2011, Southern ocean nitrogen and silicon dynamics during the last deglaciation, Earth Planet. Sci. Lett., 310, 334–339.

Jaccard, S. L., Haug, G. H., Sigman, D. M., Pedersen, T. F., Thierstein, H. R., and Röhl, U. 2005, Glacial/interglacial changes in subarctic North Pacific stratification, Science, 308, 1003–1006.

Jaccard, S. L., Galbraith, E. D., Sigman, D. M., Haug, G. H., Francois, R., Pedersen, T. F., Dulski, P., and Thierstein, H. R. 2009, Subarctic Pacific evidence for a glacial deepening of the oceanic respired carbon pool, Earth Planet. Sc. Lett., 277, 156–165.

Jaccard, S. L., E. D. Galbraith, D. M. Sigman, and G. H. Haug, 2010, A pervasive link between Antarctic ice core and subarctic Pacific sediment records over the past 800 kyrs, Quat. Sci. Rev., 29(1–2), 206–212, doi:10.1016/j.quascirev.2009.10.007.

Jang, K., Huh, Y., Han, Y., 2017, Authigenic Nd isotope record of North Pacific In-termediate Water formation and boundary exchange on the Bering Slope. Quat. Sci. Rev.156, 150–163. https://doi.org/10.1016/j.quascirev.2016 .11.032.

Katsura, S., H. Ueno, H. Mitsudera, and S. Kouketsu, 2020: Spatial distribution and seasonality of halocline structures in the subarctic North Pacific. *J. Phys. Oceanogr.*, **50**, 95–109, https://doi.org/10.1175/JPO-D-19-0133.1.

Kender, S., Ravelo, A.C., Worne, S., Swann, G.E.A., Leng, M.J., Asahi, H., Becker, J., Detlef, H., Aiello, I.W., Andreasen, D., Hall, I.R., 2018. Closure of the Bering strait caused mid-Pleistocene transition cooling. Nat. Commun. 9. https://doi.org/10. 1038/s41467-018-07828-0

Kohfeld, K. E. and Chase, Z. 2011 Controls on deglacial changes in biogenic fluxes in the North Pacific Ocean, Quaternary Sci. Rev., 30, 3350–3363.

Knudson, K.P., Ravelo, A.C., 2015a. North Pacific Intermediate Water circulation en-hanced by the closure of the Bering Strait. Paleoceanography30, 1287–1304. https://doi .org /10 .1002 /2015PA002840.

Knudson, K and Ravelo A. C. 2015b Enhanced Subarctic pacific Stratification and nutrient utilisation during glacials over the last 1.2 Myr Geophysical research letters 42 9870-9879

Kotilainen, A.T., Shackleton, N.J., 1995. Rapid climate variability in the North Pacific Ocean during the past 95,000 years. Nature 377, 323–326.

Lam, P. J., Robinson, L. F., Blusztajn, J., Li, C., Cook, M. S., Mc-Manus, J. F., and Keigwin, L. D. 2013, Transient stratification as the cause of the North Pacific productivity spike during deglaciation, Nat. Geosci., 6, 622–626, 2013.

Lattaud, J., Lo, L., Zeeden, C., Liu, Y.J., Song, S.R., van der Meer, M.T.J., Sinninghe Damsté, J.S., Schouten, S. 2019, A multiproxy study of past environmental changes in the Sea of Okhotsk during the last 1.5 Ma Org Geochem., 132, pp. 50-61

Lee, S.-Y., Poulsen, C.J., 2006. Sea ice control of Plio-Pleistocene tropical Pacific climate evolution. Earth and Planetary Science Letters 248, 238–247.

Lisiecki, L.E., Raymo, M.E., 2005. A Pliocene–Pleistocene stack of 57 globally distributed benthic d18O records. Paleoceanography 20, PA1003. http://dx.doi.org/10.1029/2004PA001071.

Max, L., Lembke-Jene, L., Riethdorf, J.R., Tiedemann, R., Nürnberg, D., Kühn, H., MacKensen, A., 2014. Pulses of enhanced north Pacific intermediate water ven-tilation from the Okhotsk Sea and Bering Sea during the last deglaciation. Clim. Past10, 591–605. https://doi .org /10 .5194 /cp -10 -591 -2014.

McCarron, A.P., Bigg, G.R., Brooks, H., Leng, M.J., Marshall, J.D., Ponomareva, V., Portnyagin, M., Reimer, J., Rogerson, M., 2021, Northwest Pacific ice-rafted debris at 38°N reveals episodic ice-sheet change in late Quaternary Northeast Siberia. Earth and Planetary Science letters 553 https://doi.org/10.1016/j.epsl.2020.116650

McClymont, E.L., Rosell-Melé, A., 2005. Links between the onset of modern Walker Circulation and the mid-Pleistocene climate transition. Geology 33, 389–392.

McClymont, E.L., Sosdian, S.M., Rosell-Melé, A., Rosenthal, Y., 2013. Pleistocene sea-surface temperature evolution: early cooling, delayed glacial intensification, and implications for the mid-Pleistocene climate transition. Earth-Sci. Rev.123, 173–193. https://doi .org /10 .1016 /j .earscirev.2013 .04 .006. McKelvey et al 1995.

Moschen, R., Lücke, A., Schleser, G., 2005. Sensitivity of biogenic silica oxygen isotopes to changes in surface water temperature and palaeoclimatology. Geophys. Res. Lett. 32, L07708. doi:10.1029/2004GL022167.

Nelson, D.M., Treguer, P., Brzezinski, M.A., Leynaert, A., Queguiner, B. 1995 Production and dissolution of biogenic silica in the ocean: revised global estimates, comparison with regional data and relationship to biogenic sedimentation Global Biogeochem. Cycles, 9, pp. 359-372.

Otosaka, S., and S. Noriki, 2005, Relationship between composition of settling particles and organic carbon flux in the western North Pacific and the Japan Sea, *J. Oceanogr.*, **61**(1), 25–40.

Panizzo, V.N., Swann, G.E.A., Mackay, A.W., Vologina, E., Sturm, M., Pashley, V., Horstwood, M.S.A., 2016. Insights into the transfer of silicon isotopes into the sediment record. Biogeosciences 13, 147–157.

Rae, James, Gray, William, Jnglin Wills, Robert, Eisenman, Ian, Fitzhugh, Ben, Fotheringham, Morag, Littley, Eloise, Rafter, Patrick, Rees-Owen, Rhian, Ridgewell, Andrew, Taylor, Ben, Burke, Andrea. 2020, Overturning circulation, nutrient limitation, and warming in the Glacial North Pacific. Science Advances. 6. eabd1654. 10.1126/sciadv.abd1654.

Rae, J. W. B., Sarnthein, M., Foster, G. L., Ridgwell, A., Grootes, P. M., and Elliott, T. 2014, Deep water formation in the North Pacific and deglacial CO2 rise, Paleoceanography, 29, 645–667, 2014.

Ravelo, A.C., Andreasen, D.H., Lyle, M., Olivarez Lyle, A., Wara, M.W., 2004. Regional climate shifts caused by gradual global cooling in the Pliocene epoch. Nature 429, 263–267.

Raymo, M.E., 1997. The timing of major climate terminations. Paleoceanography 12, 577–585.

Raymo, M.E., Lisiecki, L.E., Nisancioglu, K.H., 2006. Plio-Pleistocene ice volume, Antarctic climate, and the global {delta}18O record. Science 313, 492–495. Reynolds et al 2008

Reynolds, B. C. 2009, Modeling the modern marine δ 30Si distribution, Global Biogeochem. Cycles, 23, GB2015, doi:10.1029/2008GB003266.

Sarnthein, M., Gebhardt, H., Kiefer, T., Kucera, M., Cook, M., and Erlenkeuser, H. 2004, Mid Holocene origin of the sea-surface salinity low in the subarctic North Pacific, Quaternary Sci. Rev., 23, 2089–2099.

Shcherbina, A. Y.; L. D. Talley and D. L. Rudnick. 2003. Direct observations of North Pacific ventilation: Brine rejection in the Okhotsk Sea. Science, 302: 1952–1955.

Sigman, D. M. & Hain, M. P. 2012, The Biological Productivity of the Ocean: Section 2. *Nature Education Knowledge* 3(10):20

Sigman, D. M., Hain, M. P., & Haug, G. H. 2010. The polar ocean and glacial cycles in atmospheric CO2 concentration. Nature, 466(7302), 47–55. https://doi.org/10.1038/nature09149

Sigman, D. M., Fripiat, F., Studer, A. S., Kemeny, P. C., Martínez-García, A., Hain, M. P., Ai, X., Wang, X., ren, H., Haug. G. 2021. The Southern Ocean during the ice ages: A review of the Antarctic surface isolation hypothesis, with comparison to the North Pacific. Quaternary Science Reviews, 254, 106732

Sigman, D. M., Jaccard, S. L., & Haug, G. H. 2004. Polar ocean stratification in a cold climate. Nature, 428(6978), 59–63. https://doi.org/10.1038/nature02357

Smetacek, V. Diatoms and the ocean carbon cycle. *Protists* **150**, 25–32 1999.

St John, K.E.K., Krissek, L.A., 1999. Regional patterns of Pleistocene ice-rafted debris flux in the North Pacific. Paleoceanography 14, 653–662.

Swann, G. E. A. 2010, Salinity changes in the North West Pacific Ocean during the late Pliocene/early Quaternary from 2.73 Ma to 2.53 Ma, Earth Planet. Sc. Lett., 297, 332–338.

Swann, G. E. A., Snelling, A. M., & Pike, J., 2016. Biogeochemical cycling in the Bering Sea over the onset of major Northern Hemisphere glaciation. Paleoceanography, 31, 1261–1269. https://doi.org/10.1002/2016PA002978.

Swann, G.E.A.; Snelling, A.M. 2015 Photic zone changes in the north-west Pacific Ocean from MIS 4–5e. *Climate of the Past*, 11 (1). 15-25. https://doi.org/10.5194/cp-11-15-2015

Swann, G.E.A., Kendrick, C.P., Dickson, A.J. and Worne, S., 2018. Late Pliocene marine pCO2 reconstructions from the Subarctic Pacific Ocean Paleoceanography and Paleoclimatology. 33, 457-469

Tiedemann, R., and Haug , G. H., 1995, Astronomical calibration of cycle stratigraphy for Site 882 in the northwest Pacific, Proc. Ocean Drill. Program Sci. Results, 145, 283–292.

Tsuda, A., Takeda, S., Saito, H., Nishioka, J., Nojiri, Y., Kudo, I., Kiyosawa, H., Shiomoto, A., Imai, K., Ono, T., Shimamoto, A., Tsumune, D., Yoshimura, T., Aono, T., Hinuma, A., Kinugasa, M., Suzuki, K., Sohrin, Y., Noiri, Y., Tani, H., Deguchi, Y., Tsurushima, N., Ogawa, H., Fukami, K., Kuma, K., Saino, T., 2003. A mesoscale iron enrichment in the Western Subarctic Pacific induces a large centric diatombloom. Science 300, 958–961.

Tziperman, E., Gildor, H., 2003. On the mid-Pleistocene transition to 100-ky glacial cycles and the asymmetry between glaciation and deglaciation times. Paleoceanography 18, 1–8.

Volk, T. & Hoffert, M. I. 1985, in *The Carbon Cycle and Atmospheric CO2*: Natural Variation Archean to Present (eds E. T. Sundquist, E. T. & Broecker, W. S.) (AGU Monograph 32, American Geophysical Union, Washington DC).

Wang, Y., Zhang, H., Chen, H., & Chai, F., 2019 The sources and transport of iron in the North Pacific and its impact on marine ecosystems, Atmospheric and Oceanic Science Letters, 12:1, 30-34, DOI: 10.1080/16742834.2019.1545513

M.J. Warner, G.I. Roden, 1995 Chlorofluorocarbon evidence for recent ventilation of the deep Bering Sea Nature, 373, pp. 409-412.

Worne, S., Kender, S., Swann, G.E.A., Leng, M.J., and Ravello, A.C., 2019. Coupled climate and subarctic Pacific nutrient upwelling over the last 850,000 years. Earth and Planetary Science Letters. 522, 87 – 97.

Worne, S., Kender, S., Swann, G.E.A., Leng, M.J., and Ravello, A.C., 2020, Reduced upwelling of nutrient and carbon-rich water in the subarctic Pacific during the Mid-Pleistocene Transition. Palaeogeography, Palaeoclimatology, Palaeoecology 555 https://doi.org/10.1016/j.palaeo.2020.109845

Figures

Figure 1 [colour]: Location of ODP Site 882 and IODP Site 1341.

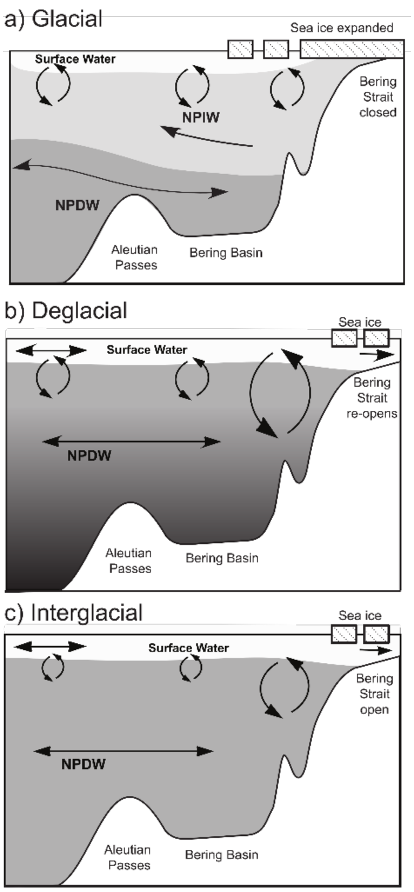

Figure 2: Schematic models representing glacial, deglacial and interglacial biogeochemical cycling between the Bering Sea and the North Pacific Ocean and the propagation of southwards of GNPIW. Modified from Kender et al 2018 and Worne et al 2019.

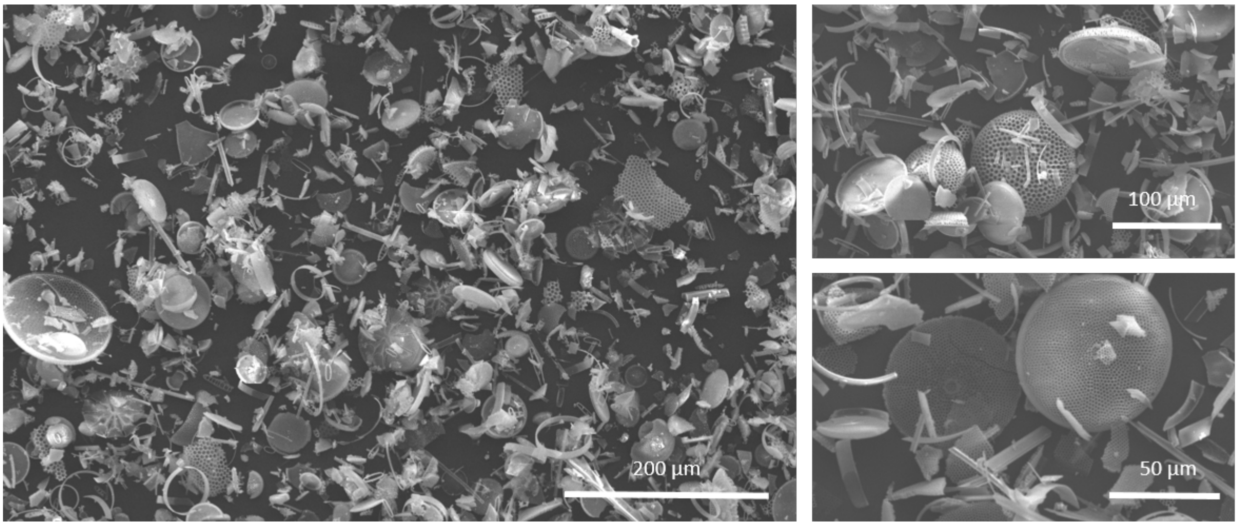

Figure 3: Scanning electron microscope (SEM) images of clean diatom samples from ODP Site 882.

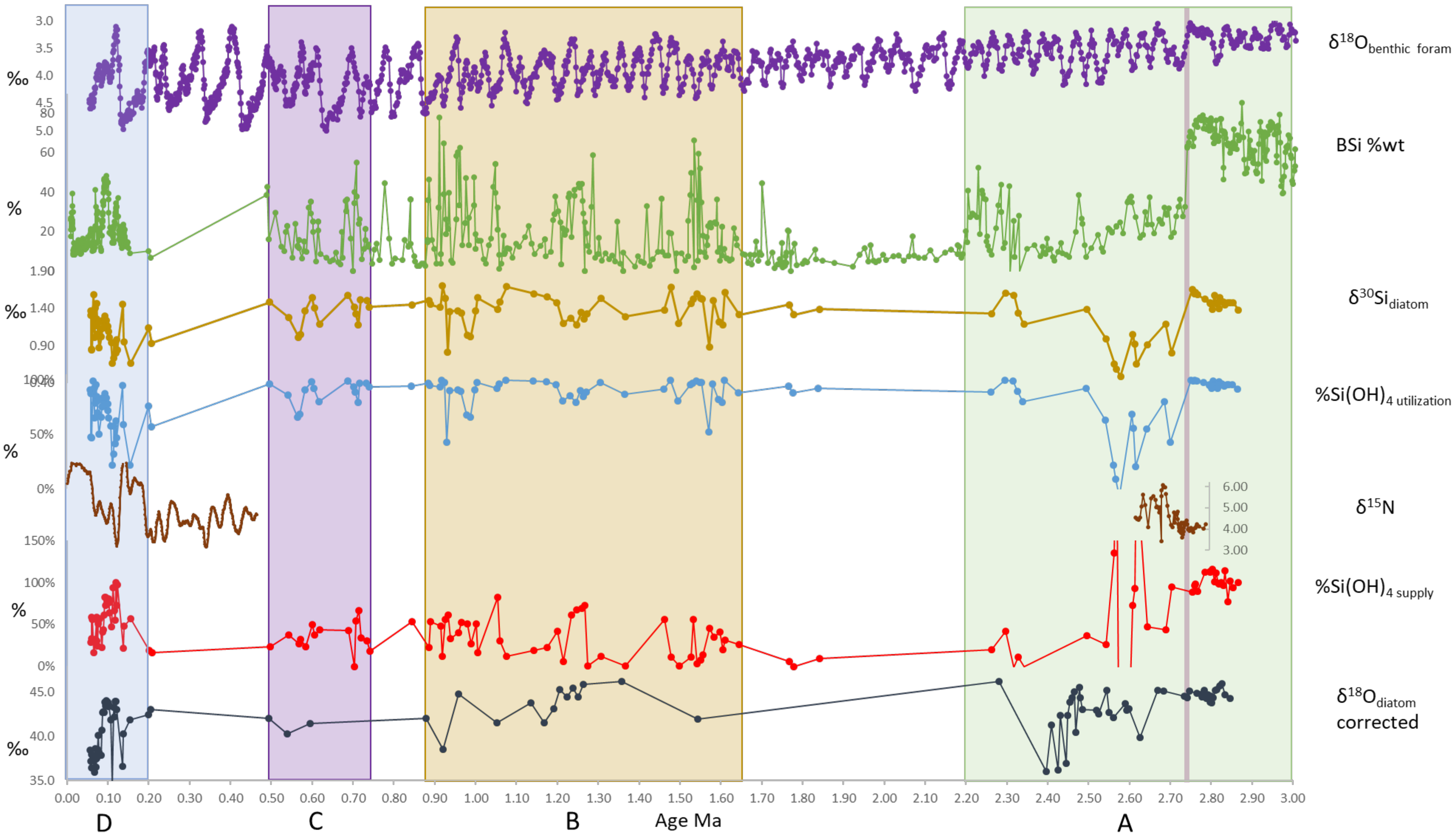
δ18Obenthic foram
BSi %wt
δ30Sidiatom
%Si(OH)4 utilization
δ15N
%Si(OH)4 supply
δ18Odiatom corrected
‰
%
‰
%
%
‰
3.0
3.5
4.0
4.5
5.0
80
60
40
20
1.90
1.40
0.90
0.40
100%
50%
0%
150%
100%
50%
0%
45.0
40.0
35.0
6.00
5.00
4.00
3.00
0.00 0.10 0.20 0.30 0.40 0.50 0.60 0.70 0.80 0.90 1.00 1.10 1.20 1.30 1.40 1.50 1.60 1.70 1.80 1.90 2.00 2.10 2.20 2.30 2.40 2.50 2.60 2.70 2.80 2.90 3.00
D
C
B
Age Ma
A

Figure 4 [colour]: Data from ODP Site 882 showing changes in the LR04 benthic foraminifera $\delta^{18}O$ record ($\delta^{18}O_{benthic\ foram.}$) (Lisecki and Raymo 2004), opal concentration (BSi %wt) (Swann 2010, Bailey et al., 2011, Swann and Snelling 2015), $\delta^{30}Si_{diatom}$, nutrient consumption (%$Si(OH)_{4\ utilisation}$), $\delta^{15}N_{bulk}$ (0-0.5 Ma Galbraith et al., 2008; 2.6-2.8 Ma Studer et al., (2012; pers comm.)) nutrient supply (%$Si(OH)_{4\ supply}$) and fresh water input ($\delta^{18}O_{diatom}$ corrected). Shaded areas relate to sections discussed in the text. Purple line at 2.73 Ma marks NHG.

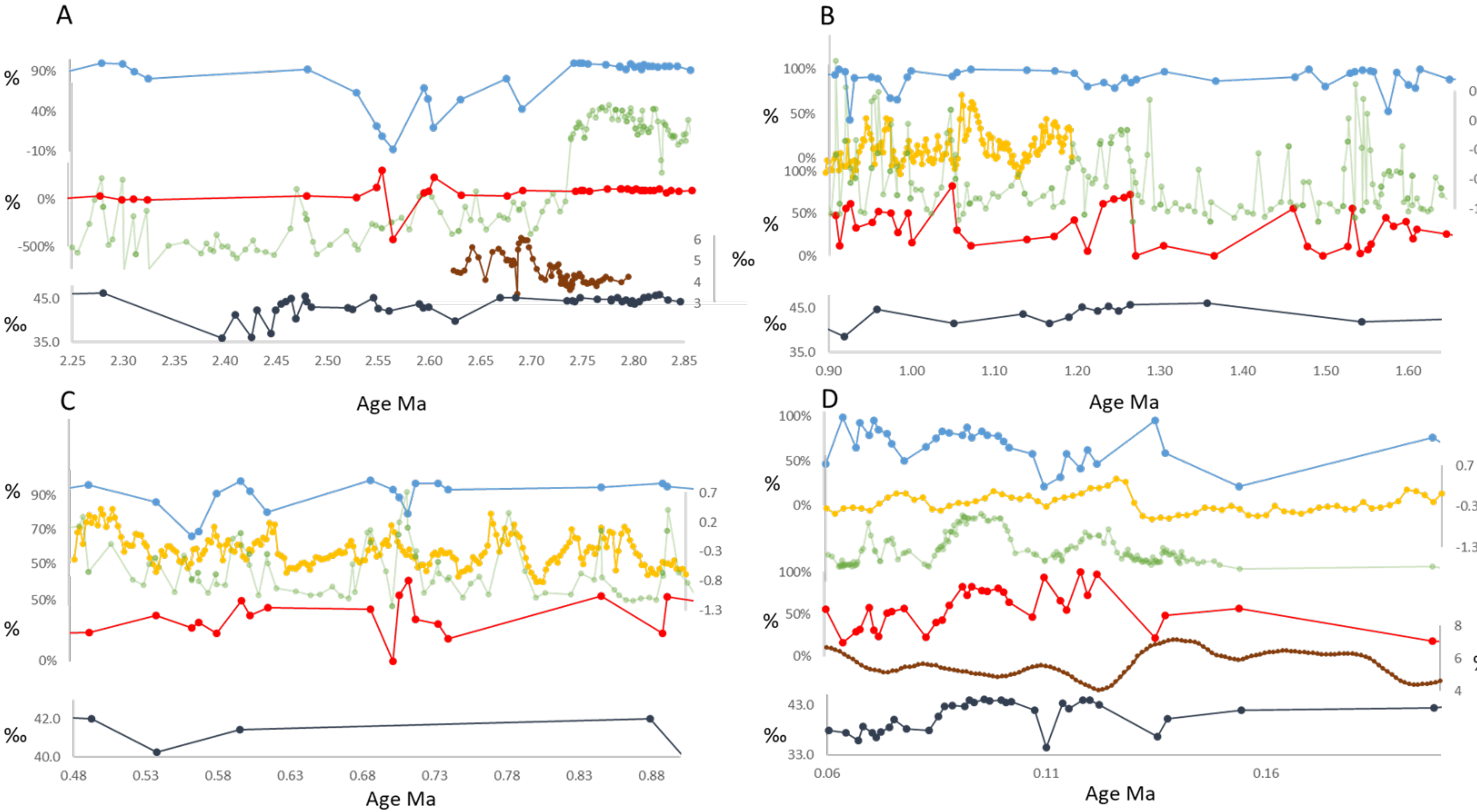

740

Figure 5A-D [colour]: Detailed Data from ODP Site 882 showing changes in the opal concentration (BSi %wt), nutrient consumption (%$Si(OH)_{4\ utilisation}$), nutrient supply (%$Si(OH)_{4\ supply}$) and fresh water input ($\delta^{18}O_{diatom}$ corrected). The Bering Sea upwelling index (Worne et al 2019) is shown where data is available as is $\delta^{15}N$ from Studer et al., (2.8-2.6 Ma) (2012., pers comm.) and Galbraith 2008 (0.06-2 Ma) (BSi %wt is shown in the background in green). Purple line at 2.73 Ma marks NHG.